sciendo

ARTIFICIAL SATELLITES, Vol. 58, No. 4 – 2023
DOI: 10.2478/arsa-2023-0012

EVALUATION OF TRIPLE-FREQUENCY GPS/GALILEO/BEIDOU KINEMATIC PRECISE POINT POSITIONING USING REAL-TIME CNES PRODUCTS FOR MARITIME APPLICATIONS

Mohamed ABDELAZEEM[1,2], Rahmi N. ÇELIK [3]

[1] Civil Engineering Department, College of Engineering, Prince Sattam Bin Abdulaziz University, Saudi Arabia
[2] Civil Engineering Department, Faculty of Engineering, Aswan University, Egypt
[3] Geomatics Engineering Department, Istanbul Technical University, Turkey

e-mails: moh.azm84@gmail.com, celikn@itu.edu.tr

ABSTRACT. Our research aims to evaluate the triple-frequency GPS/Galileo/BeiDou kinematic precise point positioning (PPP) accuracy for the international maritime organization (IMO) positioning accuracy and integrity requirements. The real-time Centre National d'Etudes Spatiales (CNES) satellite orbit and clock products are used to simulate real-time scenarios. GPS/Galileo/BeiDou observations are collected from a moving vessel. Both dual-frequency and triple-frequency ionosphere-free PPP models are developed. Different satellite system combinations are used, including GPS-only, GPS/Galileo, GPS/BeiDou, and GPS/Galileo/BeiDou. The GPS-only differential solution is used as a reference. It is found that both dual- and triple-frequency kinematic PPP solutions achieve the IMO accuracy requirements at 95% confidence level for ocean, coastal, port approach, port, inland waterways, and track control navigation applications, except the automatic docking application. Moreover, the PPP solutions fulfilled the IMO integrity requirements for all navigation phase applications, but the GPS and GPS/BeiDou PPP solutions did not fulfill the automatic docking integrity requirement.

Keywords: triple-frequency, GPS/Galileo/BeiDou, CNES real-time products, maritime applications, International Maritime Organization (IMO)

1. INTRODUCTION

The global navigation satellite systems (GNSS) have been widely used over the last decades in precise navigation, hydrographic survey, and maritime applications. There are different GNSS positioning techniques that can be used in maritime navigation, including differential, real-time kinematic (RTK), and precise point positioning (PPP) techniques. The maritime accuracy requirements for navigation and positioning are specified by the International Maritime Organization (IMO) standards (i.e., IMO resolution A.915 (IMO, 2002). Maritime navigation consists of a number of phases, including ocean, coastal, port approach and restricted waters, port, inland waterways, track control, and automatic docking. For maritime navigation, the

©The Author(s). This is an open-access article distributed under the terms of the Creative Commons Attribution License (CC BY 4.0, https://creativecommons.org/licenses/by/4.0/), which permits use, distribution, and reproduction in any medium, provided that the Article is properly cited.

positioning error should be estimated at 95% confidence level. The positioning accuracy requirements of each maritime navigation phase are given in Table 1.

Table 1. IMO accuracy requirements for GNSS positioning (IMO, 2002)

Navigation phase	Horizontal accuracy (m)	Integrity		
		Alert limit (m)	Time to alarm (seconds)	Integrity risk (per 3 h)
Ocean	10	25	10	10^{-5}
Coastal	10	25	10	10^{-5}
Port approach	10	25	10	10^{-5}
Inland waterways	10	25	10	10^{-5}
Track control	10	25	10	10^{-5}
In port navigation	1	2.5	10	10^{-5}
Automatic docking	0.1	0.25	10	10^{-5}

The performance of the kinematic GNSS PPP solution in hydrographic and maritime applications has been investigated by a number of researchers (e.g., Alkan and Ocalan, 2013; El-Diasty and Elsobeiey, 2015; Berber and Wright, 2016; El-Diasty, 2016; Akpınar and Aykut, 2017; Alkan et al., 2017; Tegedor et al., 2017; Farah 2018; Specht et al., 2019; Yang et al., 2019; Erol 2020; Erol et al., 2020; Alkan et al., 2020; Nie et al., 2020; Tunalioglu et al., 2022). Yang et al. (2019) investigated the accuracy of the GPS/GLONASS/BeiDou RTK PPP solution for maritime applications. The accuracies of single constellation (i.e., GPS-only and BeiDou-only) and multi-constellation (i.e., GPS/BeiDou, GPS/GLONASS, GLONASS/BeiDou, and GPS/GLONASS/BeiDou) have been examined. The network RTK solution has been used as a reference. It was shown that the accuracy of the proposed real-time PPP solutions was within decimeter level. In addition, the accuracy of the GPS/BeiDou solution was superior to the GPS/GLONASS, GLONASS/BeiDou solutions. Erol (2020) examined the performance of multi-GNSS kinematic PPP solution using precise satellite orbit and clock products from different international GNSS service (IGS) analysis centers for marine applications. The carrier phase–based differential kinematic solution was used as a reference. It was found that the GPS/GLONASS/Galileo/BeiDou PPP solution using the German research center for geosciences (GFZ) products provided better accuracy than the other PPP solutions.

Presently, triple-frequency GPS/Galileo/BeiDou observations have become available, which in turn provide redundant measurements, various linear combinations, and fast ambiguity resolution (AR). Therefore, the PPP solution is enhanced particularly the convergence time. However, the satellite and receiver inter-frequency biases (IFB) are added as additional unknown parameters. IFB include phase and code biases. The phase IFB is the difference between the L_1/L_2 clock and the L_1/L_5 clock combinations, while the code IFB is the difference between differential code biases (DCB) estimated from $P_1–P_2$ and $P_1–P_5$ combinations. The ionosphere-free triple-frequency PPP solution can be executed using different models including two dual-frequency combinations (i.e., IF_{12} and IF_{13}), a triple-frequency combination (i.e., IF_{123}), between-satellite single-difference (BSSD) and semi-decoupled models.

The accuracy of the triple-frequency GNSS PPP has been examined in a number of studies (e.g., Cao et al., 2019; Pan et al., 2019; Geng et al., 2020; Li et al., 2020; Abd Rabbou et al., 2021; Guo et al., 2021; Naciri and Bisnath, 2021). Pan et al. (2019) evaluated the accuracy of three static triple-frequency GPS PPP solutions, which are two dual-frequency ionosphere-free combinations (i.e., L_1/L_2 and L_2/L_5) PPP, triple-frequency ionosphere-free PPP and triple-

frequency uncombined PPP solutions. It was shown that comparable positioning accuracy was obtained from the three solutions. The convergence time of the triple-frequency ionosphere-free solution was better than the two solutions. Abd Rabbou et al. (2021) developed new triple-frequency GPS/Galileo PPP processing models, including undifferenced, BSSD, and semi-decoupled models. In addition, the traditional ionosphere-free dual-frequency PPP model has been used. The models developed by them have been validated for static and kinematic applications. It has been found that the positioning accuracy and convergence time of the triple-frequency PPP solutions have been improved compared to the undifferenced dual-frequency PPP solution. Furthermore, the performance of the triple-frequency semi-decoupled PPP model was superior to the other developed models.

Currently, a reliable real-time PPP solution can be obtained by using the IGS real-time service (RTS) products. RTS products include satellite orbit and clock corrections, code and phase biases, as well as vertical total electron contents (VTECs), which are available from a number of analysis centers. The Centre National d'Etudes Spatiales (CNES) provides real-time products for GPS, GLONASS, Galileo, and BeiDou satellite systems into two forms: the post processed and real-time streams (i.e., CLK 92 and CLK 93). A number of researchers have investigated the performance of the CNES real-time products (e.g., Wang et al., 2018; Katsigianni et al., 2019; Kazmierski et al., 2020; Nie et al., 2020; Wang et al., 2020; Zhao et al., 2020; Chen et al., 2021; Elmezayen and El-Rabbany 2021).

The objective of our study is to investigate the accuracy of kinematic triple-frequency GPS/Galileo/BeiDou PPP solution for maritime applications. Real-time CNES satellite orbit and clock products are used. GPS/Galileo/BeiDou measurements from a moving vessel are collected and then processed using two PPP models, which are the dual-frequency ionosphere-free PPP and the triple-frequency ionosphere-free PPP. The collected observations are also processed using different satellite combinations, namely GPS-only, GPS/Galileo, GPS/BeiDou, and GPS/Galileo/BeiDou. GPS differential solution is used as a reference. The estimated positioning accuracies are validated with respect to the minimum IMO positioning accuracy and integrity requirements for maritime applications.

2. GNSS PPP MATHEMATICAL MODELS

The basic GNSS observation equation for pseudorange and carrier phase observations can be expressed as follows (Hofmann-Wellenhof et al., 2008):

$$P_i^s = \rho_r^s + c(dt_r - dt^s) + I_{r,i}^s + T_r^s + c\left(B_{r,i} - B_i^s\right) + \varepsilon_{P,i} \tag{1}$$

$$\Phi_i^s = \rho_r^s + c(dt_r - dt^s) - I_{r,i}^s + T_r^s + c\left(\delta_{r,i} - \delta_i^s\right) + \lambda_i N_{r,i}^s + \varepsilon_{\Phi,i} \tag{2}$$

where i, s and r refer to frequency, GNSS satellite and receiver, respectively; P and Φ are the pseudorange and carrier phase observations, respectively; ρ_r^s is the satellite-receiver true geometric range; c is the speed of light in vacuum; dt_r and dt^s are the receiver and satellite clock errors, respectively; $I_{r,i}^s$ is the ionospheric delay; T_r^s is the tropospheric delay, which is divided into hydrostatic and wet components; $B_{r,i}$ and B_i^s are the code hardware delays for both receiver and satellite, respectively; $\delta_{r,i}$ and δ_i^s are the phase hardware delays for both receiver and satellite, respectively; λ_i is the carrier phase wavelength; $N_{r,i}^s$ is the non-integer ambiguity parameter; $\varepsilon_{P,i}$ and $\varepsilon_{\Phi,i}$ are the code and phase unmodeled residual errors, respectively.

2.1. Dual-frequency ionosphere-free PPP model

The mathematical expression of the dual-frequency ionosphere-free PPP for pseudorange and carrier phase observables can be written as follows (Hofmann-Wellenhof et al., 2008):

$$P_{IF} = \rho_r^s + c(dt_r - dt^s) + T_r^s + c(\Delta B_r - \Delta B^s) + \varepsilon_{P,IF} \quad (3)$$

$$\Phi_{IF} = \rho_r^s + c(dt_r - dt^s) + T_r^s + c(\Delta \delta_r - \Delta \delta^s) + \overline{\lambda N_r^s} + \varepsilon_{\Phi,IF} \quad (4)$$

where P_{IF} and Φ_{IF} are the dual-frequency ionosphere-free linear combination of pseudorange and carrier phase observations, respectively; ΔB_r and ΔB^s are the ionosphere-free DCB for receiver and satellite, respectively; $\Delta \delta_r$ and $\Delta \delta^s$ are the ionosphere-free differential phase bias for receiver and satellite, respectively; $\overline{\lambda N_r^s}$ is the non-integer ambiguity term for phase observations, which takes the following form based on the frequencies f_1 and f_2 of L_1 and L_2 signals, respectively:

$$\overline{\lambda N_r^s} = \left(\frac{f_1^2 \lambda_1 N_{r,1}^s - f_2^2 \lambda_2 N_{r,2}^s}{f_1^2 - f_2^2} \right) \quad (5)$$

In the dual-frequency ionosphere-free PPP model, DCB is lumped into the satellite clock errors and the receiver clock errors. After using the precise satellite clock products, the PPP model using GPS, Galileo and BeiDou observations can written as follows:

$$P_{IF}^G = \rho_r^G + c\left(dt_{r,G} + \Delta B_{r,G}\right) - c\left(dt_{prec}^G + \Delta B^G\right) + T_r^G + \varepsilon_P^G \quad (6)$$

$$\Phi_{IF}^G = \rho_r^G + c\left(dt_{r,G} + \Delta B_{r,G}\right) - c\left(dt_{prec}^G + \Delta B^G\right) + T_r^G + \left(\overline{\lambda N_r^G} + D_{G,r} - D^G\right) + \varepsilon_\Phi^G \quad (7)$$

$$P_{IF}^J = \rho_r^J + c\left(dt_{r,G} + \Delta B_{r,G}\right) - c\left(dt_{prec}^J + \Delta B^J\right) + T_r^J + ISB^J + \varepsilon_P^J \quad (8)$$

$$\Phi_{IF}^J = \rho_r^J + c\left(dt_{r,G} + \Delta B_{r,G}\right) - c\left(dt_{prec}^J + \Delta B^J\right) + T_r^J + ISB^J + \left(\overline{\lambda N_r^J} + D_{J,r} - D^J\right) + \varepsilon_\Phi^J \quad (9)$$

where G and J refer to the GPS and other GNSS systems (i.e., Galileo and BeiDou), respectively; dt_{prec}^G and dt_{prec}^J are the precise satellite clock parameters for GPS and other GNSS systems, respectively; D_r is the difference between the receiver differential code and phase biases; D^G and D^J are the differences between the satellite differential code and phase biases for GPS and other GNSS systems, respectively; ISB^J is the inter-system bias (ISB), including the difference between the receiver DCB for GPS and other satellite systems.

The unknown parameters for the dual-frequency ionosphere-free PPP solution can take the following mathematical expression:

$$\boldsymbol{X} = \left[\Delta x \quad \Delta y \quad \Delta z \quad cdt_{r,G} \quad zwd \quad ISB^J \quad \widetilde{N_G^1} \quad \ldots \quad \widetilde{N_G^{n_G}} \quad \widetilde{N_j^1} \quad \cdots \quad \widetilde{N_J^{n_J}}\right]^T \quad (10)$$

where $\boldsymbol{X}$ is the vector of the unknown parameters; Δx, Δy and Δz represent the receiver coordinate corrections; zwd denotes the wet component of zenith tropospheric delay; n_G is the number of visible GPS satellites; n_J is the number of other visible GNSS satellites; $\widetilde{N}$ represents the ambiguity parameter (i.e., $\widetilde{N} = \overline{\lambda N_r^s} + D_r - D^s$).

2.2. Triple-frequency ionosphere-free PPP model

The triple-frequency ionosphere-free PPP model can be formed using two dual-frequency ionosphere-free linear combinations (i.e., IF12 and IF13) of pseudorange and carrier phase observations as follows (Guo et al., 2016):

$$P_{IF,12}^G = \rho_r^G + cdt_{r,G,12} - cdt_{prec,12}^G + c\Delta B_{r,G,12} - c\Delta B_{12}^G + T_r^G + \varepsilon_{P,12}^G \quad (11)$$

$$P_{IF,13}^{G} = \rho_r^G + cdt_{r,G,12} - cdt_{prec,12}^{G} - c\Delta B_{13}^{G} + T_r^G + IFB^G + \varepsilon_{P,13}^{G} \quad (12)$$

$$\Phi_{IF,12}^{G} = \rho_r^G + cdt_{r,G,12} - cdt_{prec,12}^{G} + T_r^G + \left(\overline{\lambda N_{r,12}^{G}} + D_{G,r,12} - D_{12}^{G}\right) + \varepsilon_{\Phi,12}^{G} \quad (13)$$

$$\Phi_{IF,13}^{G} = \rho_r^G + cdt_{r,G,12} - cdt_{prec,12}^{G} + T_r^G + \left(\overline{\lambda N_{r,13}^{G}} + D_{G,r,13} - D_{13}^{G} + IFB^G\right) + \varepsilon_{\Phi,13}^{G} \quad (14)$$

$$P_{IF,12}^{J} = \rho_r^J + cdt_{r,G,12} - cdt_{prec,12}^{J} + c\Delta B_{r,J,12} - c\Delta B_{12}^{J} + T_r^J + ISB_{12}^{J} + \varepsilon_{P,12}^{J} \quad (15)$$

$$P_{IF,13}^{J} = \rho_r^J + cdt_{r,G,12} - cdt_{prec,12}^{J} - c\Delta B_{13}^{J} + T_r^J + IFB^J + ISB_{13}^{J} + \varepsilon_{P,13}^{J} \quad (16)$$

$$\Phi_{IF,12}^{J} = \rho_r^J + cdt_{r,G,12} - cdt_{prec,12}^{J} + T_r^J + ISB_{12}^{J} + \left(\overline{\lambda N_{r,12}^{J}} + D_{J,r,12} - D_{12}^{J}\right) + \varepsilon_{\Phi,12}^{J} \quad (17)$$

$$\Phi_{IF,13}^{J} = \rho_r^J + cdt_{r,G,12} - cdt_{prec,12}^{J} + T_r^J + ISB_{13}^{J} + \left(\overline{\lambda N_{r,13}^{J}} + D_{J,r,13} - D_{13}^{J} + IFB^J\right) + \varepsilon_{\Phi,12}^{J} \quad (18)$$

where $P_{IF,12}^{G}$ and $P_{IF,13}^{G}$ are the L_1/L_2 and L_1/L_3 ionosphere-free combinations using GPS pseudorange observations, respectively; $P_{IF,12}^{J}$ and $P_{IF,13}^{J}$ are the L_1/L_2 and L_1/L_3 ionosphere-free combinations using other GNSS systems' pseudorange observations, respectively; $\Phi_{IF,12}^{G}$ and $\Phi_{IF,12}^{J}$ are the L_1/L_2 carrier phase ionosphere-free combinations for GPS and other satellite systems, respectively; $\Phi_{IF,13}^{G}$ and $\Phi_{IF,13}^{J}$ are the L_1/L_3 carrier phase ionosphere-free combinations for GPS and other satellite systems, respectively; IFB^G and IFB^J are IFBs for GPS and other satellite systems, respectively; ISB_{12}^{J} and ISB_{13}^{J} are ISBs for L_1/L_2 and L_1/L_3 combinations, respectively.

It can be seen that both receiver and satellite clock parameters are estimated for L_1/L_2 ionosphere-free combination. In addition, DCB are not lumped into receiver and satellite clock parameters. This is because DCBs are different on each ionosphere-free combination. Therefore, an IFB parameter, known as inter-frequency clock bias (IFCB), is introduced on IF_{13} combination. For code observations, the IFB parameter is the difference between ionosphere-free receiver DCB_{12} and DCB_{13} ($IFB = \Delta B_{r,12} - \Delta B_{r,13}$), while it is lumped into the ambiguity term for carrier phase observations. Moreover, the satellite DCB can be estimated using the IGS multi-GNSS experiment (MGEX) products.

As a result, the vector of the parameter estimates can be expressed mathematically as follows:

$$\boldsymbol{X} = \left[\Delta x \quad \Delta y \quad \Delta z \quad cdt_{r,G12} \quad zwd \quad ISB_{12}^{J} \quad ISB_{13}^{J} \quad IFB \quad \widetilde{N_G^1} \quad \ldots \quad \widetilde{N_G^{n_G}} \quad \widetilde{N_J^1} \quad \cdots \quad \widetilde{N_J^{n_J}}\right]^T \quad (19)$$

where $dt_{r,G12}$ indicates the GPS receiver clock parameter for L_1/L_2 ionosphere-free combination.

3. KINEMATIC DATA SET

To assess the performance of the kinematic PPP solution for maritime applications, a kinematic trajectory was observed in Bosporus, Istanbul, Turkey. The vessel trajectory is shown in Figure 1. A multi-frequency multi-GNSS Leica GS15 receiver had been located onboard the vessel to collect the observations with 1-s interval. The duration of the kinematic data set was about 11,298 s (about 3.18 h). The base station PALA of the Istanbul water and sewerage administration (ISKI) continuously operating reference stations network has been used as a reference station. Static GPS observations at the reference station have been simultaneously collected and processed using the differential solution, which has been used as the reference solution.

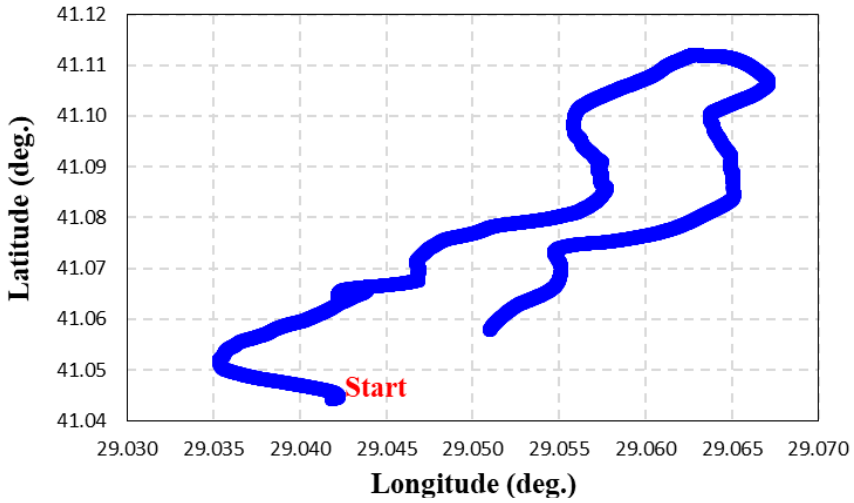

Figure 1. Vessel trajectory

Figure 2 illustrates the number of tracked satellites and their position dilution of precision (PDOP) values. It can be seen that the combined GPS/Galileo/BeiDou (GEC) system provides more tracked satellites and improves the PDOP values. In addition, the PDOP values of the combined GPS/Galileo (GE) system are better than those of the GPS/BeiDou (GC) and GPS (G) systems.

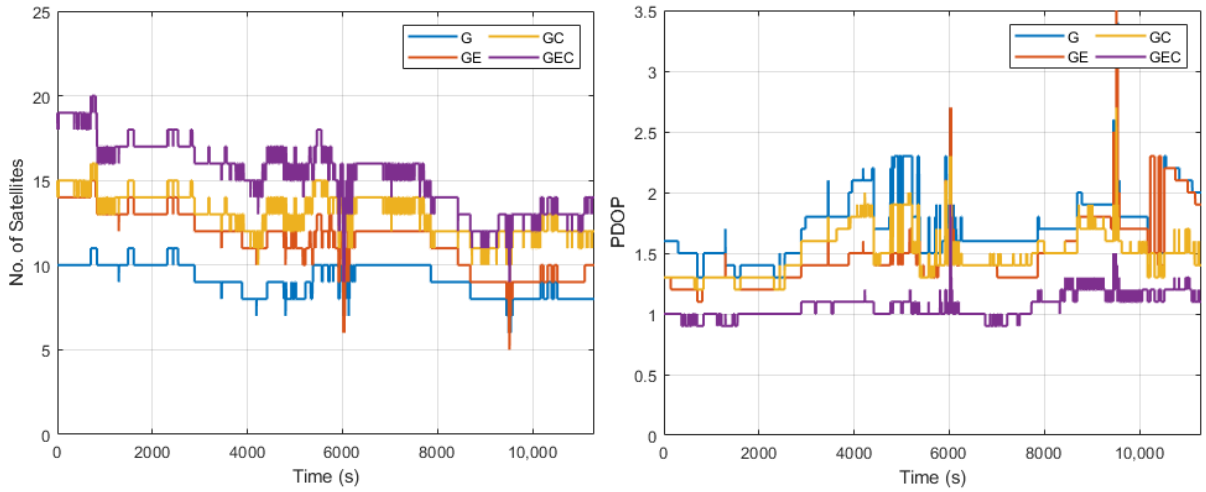

Figure 2. Number of tracked satellites (left) and PDOP values (right)

To process the collected observations, Net_Diff GNSS software (Zhang et al., 2020) has been used. Net_Diff software can process multi-frequency multi-GNSS observations using different solutions, including single point positioning (SPP), PPP, PPP AR, differential, RTK, and RTK-PPP. For the orbit file, the SP3, broadcast, and state space representation (SSR) corrections formats can be used as well as for the clock file. In addition, the standard data formats including RINEX, EOP, ATX, DCB, and BSX can be imported. For data processing, the software applies different tropospheric delay correction, mapping functions, cycle slip, data smoothing, data combination, and parameter estimation models. It also provides various processing outputs, including coordinate comparison, cycle slip, ionosphere, troposphere, observation minus correction, and positioning residuals. In addition, several plots (e.g., coordinate plots, satellite number, satellite sky view, and satellite visibility) are provided.

Our kinematic trajectory data set has been processed using dual-frequency ionosphere-free, and triple-frequency ionosphere-free kinematic PPP solutions. To validate the accuracy of the

obtained kinematic PPP solutions, the GPS observations from both the onboard vessel and the reference station have been processed using the post processed kinematic differential solution available in the Net_Diff software. The real-time CNES products (CNES, 2023) have been used to account for the satellite orbit and clock errors for PPP solution, while the final IGS products (IGS, 2023) have been used for the differential solution. The processing parameters of each solution are summarized in Table 2.

Table 2. Processing parameters for both PPP and differential solutions

Parameter	PPP solution		Differential solution
	Dual frequency	Triple frequency	
GNSS system	G, E, C	G, E, C	G
Observations	Code and phase	Code and phase	Code and phase
Mathematical model	Undifferenced ionosphere-free	Undifferenced ionosphere-free	Differenced
Frequency	G: L_1/L_2 E: E_1/E_{5a} C: B_1/B_2	G: $L_1/L_2/L_5$ E: $E_1/E_{5a}/E_{5b}$ C: $B_1/B_2/B_3$	L_1/L_2
Sampling rate	1 Hz	1 Hz	1 Hz
Elevation mask	10°	10°	10°
Orbit and clock	CNES (RT)	CNES (RT)	IGS (final)
Tropospheric model	Saastamoinen model		
Mapping function	Vienna mapping function 1 (VMF-1)		
Parameter estimation	Kalman filter		

4. RESULTS AND ANALYSIS

To investigate the accuracy of the developed kinematic PPP models using CNES real-time satellite orbits and clock products, different GNSS combinations are used, including GPS (G), GPS/Galileo (GE), GPS/BeiDou (GC), and GPS/Galileo/BeiDou (GEC). Furthermore, the aforementioned GNSS combinations are processed using two models namely, undifferenced dual-frequency ionosphere-free PPP (i.e., G-DF, GE-DF, GC-DF and GEC-DF) and undifferenced triple-frequency ionosphere-free PPP (i.e., G-TF, GE-TF, GC-TF and GEC-TF). Then, the estimated coordinates from all PPP solutions are compared with those obtained through the differential solution.

Figures 3 and 4 show the positioning errors in longitude, latitude, and altitude components, respectively, for the dual-frequency ionosphere-free and the triple-frequency ionosphere-free kinematic PPP solutions. As can be seen in the figures, the kinematic PPP solutions show very less decimeter-level positioning accuracy. Improvement in accuracy of the kinematic PPP solutions in the three components is obtained by adding Galileo and BeiDou observations to the GPS-only solution. In addition, the latitude positioning accuracy is superior to the other positioning components. This can be attributed to the GNSS satellite configuration. Furthermore, the accuracy of the triple-frequency ionosphere-free PPP solution is better than the dual-frequency PPP in longitude, latitude, and height components. It is also shown that the triple-frequency ionosphere-free PPP model converges faster than the dual-frequency PPP model. This is because the triple-frequency ionosphere-free PPP model provides redundant observations and thus more linear combinations than the traditional dual-frequency solution.

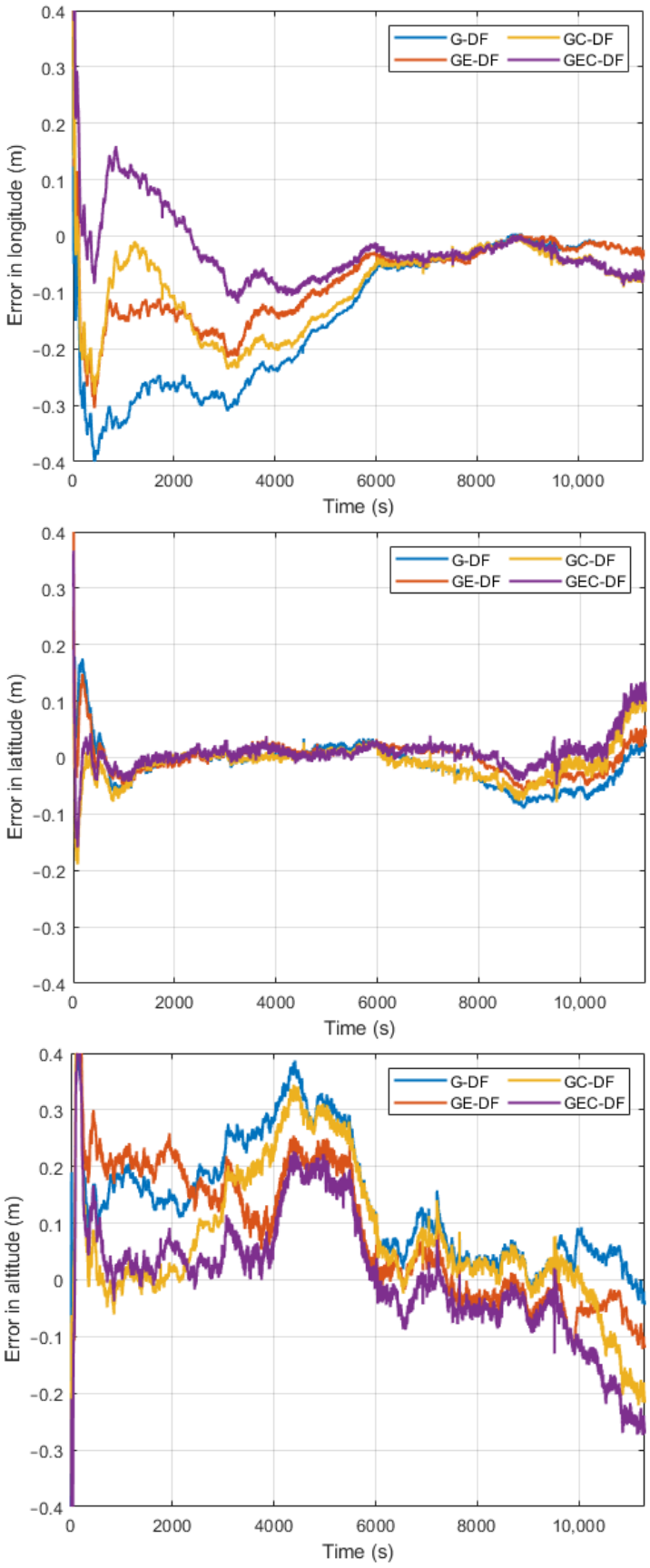

Figure 3. Positioning errors in longitude, latitude, and altitude, respectively, for dual-frequency real-time PPP solutions

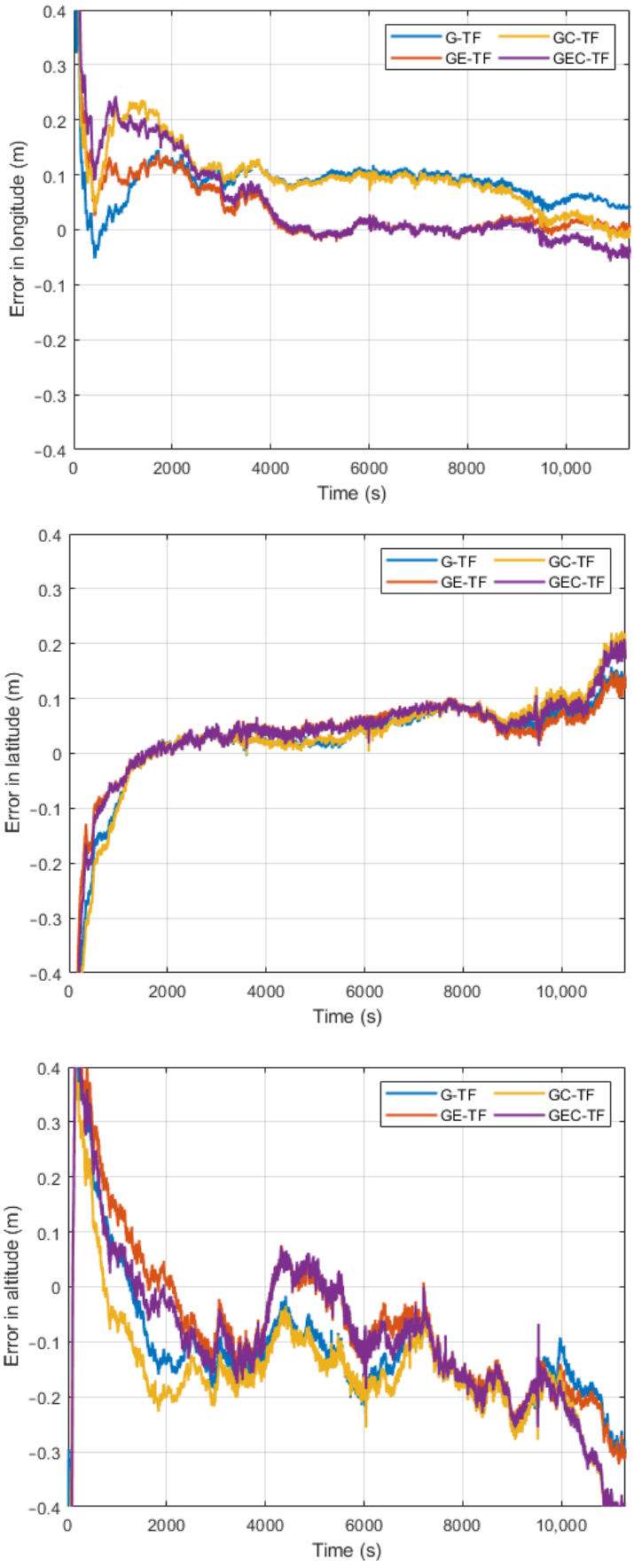

Figure 4. Positioning errors in longitude, latitude, and altitude, respectively, for triple-frequency real-time PPP solutions

The PPP positioning accuracy is also investigated through computation of the differences with respect to the differential solution in longitude, latitude, and altitude components. Figures 5 and 6 illustrate the distribution of the differences for the dual-frequency PPP and triple-frequency PPP solutions, respectively. It can be noticed that the differences are in ±10 cm level for both longitude and latitude components, while it is in ±20 cm level for the height component. Moreover, the distribution of the height component for the triple-frequency PPP solutions is better than that of the dual-frequency PPP solutions. Furthermore, distribution of latitude differences is better than that of the longitude component. This may be due to the satellite distribution geometry.

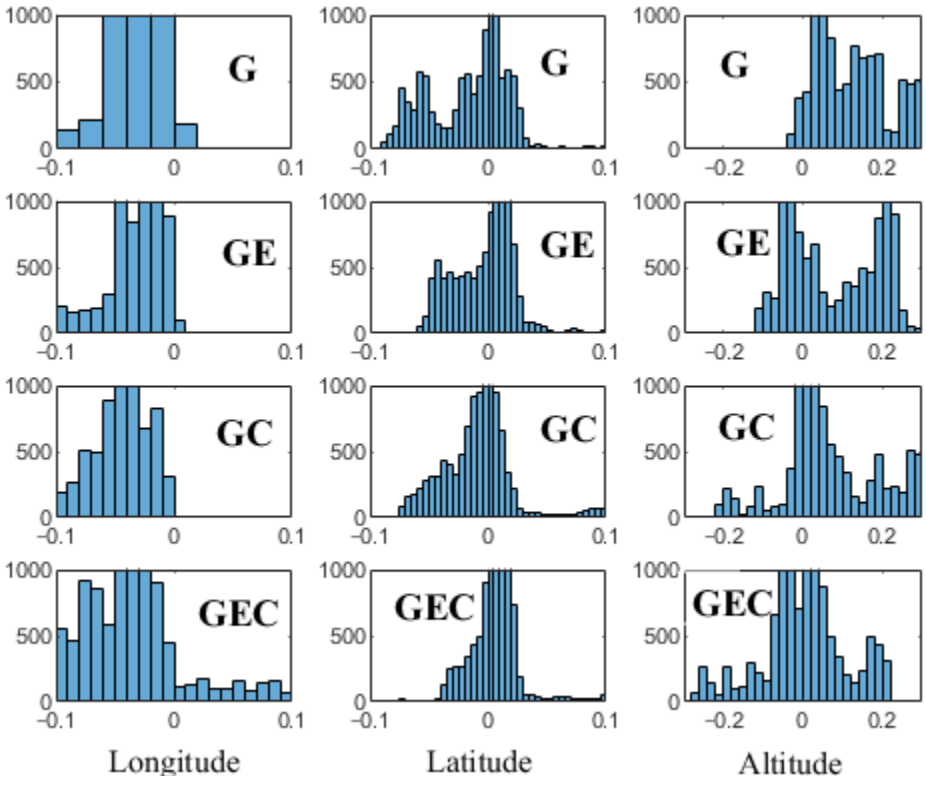

Figure 5. Distribution of the differences between the dual-frequency PPP solutions and the differential solution in the three components

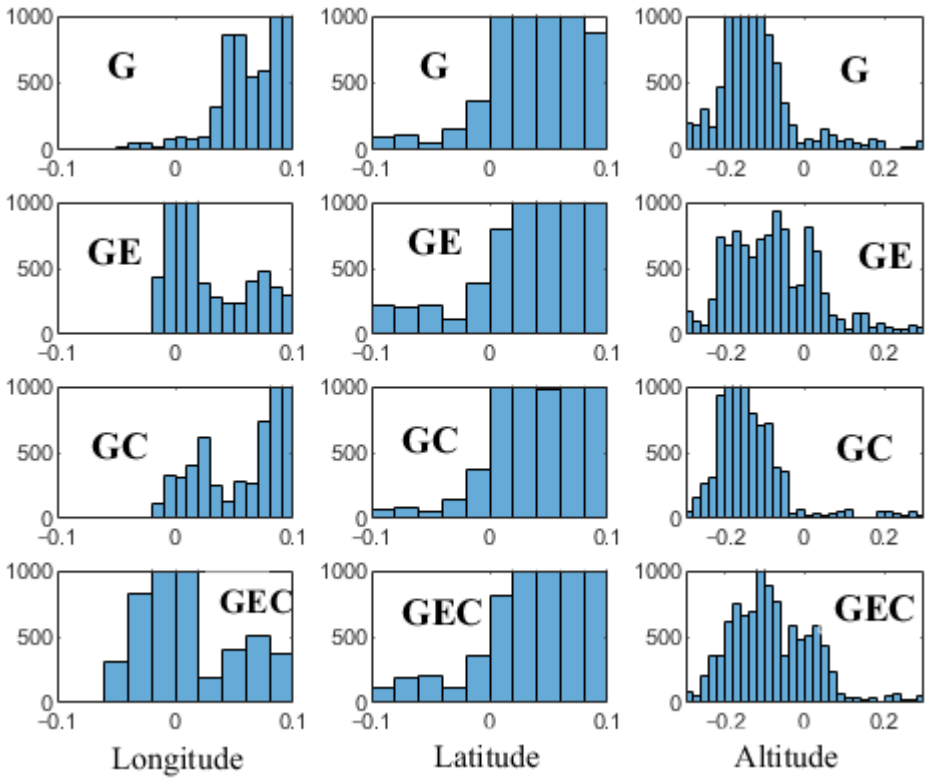

Figure 6. Distribution of the differences between the triple-frequency PPP solutions and the differential solution in the three components

To evaluate the precision of the PPP solutions, the standard deviation (STD) of the differences in longitude, latitude, and altitude components is computed (Figure 7). It can be seen that the maximum STD value is less than 0.12 m in longitude, latitude, and altitude components. In addition, the precision of the triple-frequency ionosphere-free PPP solutions is enhanced compared to that of the dual-frequency ionosphere-free PPP solutions.

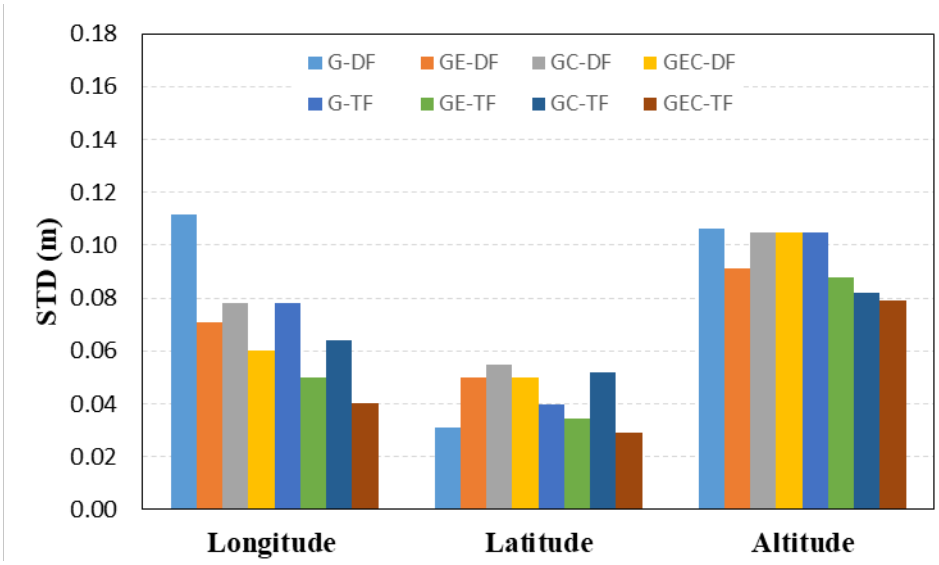

Figure 7. STD of the PPP solutions in the three positioning components

To further assess the precision of triple-frequency PPP solutions, STD of the two-dimensional (2D) and three-dimensional (3D) positioning differences are computed and it is presented in Figure 8. It is clear that the 2D STD values are less than 0.12 m, while the 3D STDs are less

than 0.16 m for the proposed PPP scenarios. Moreover, adding the third frequency to the PPP solution obviously improves the 2D or 3D positioning precision compared to the dual-frequency solution. This can be attributed to observations and linear combination redundancy. For the GPS-only solution, as an example, 2D STD is enhanced from 0.12 to 0.09 m, while 3D STD is improved from 0.16 to 0.14 m for the G-TF and G-DF solutions, respectively. Additionally, 2D and 3D STD of the GE-TF solution is reduced from 0.09 to 0.06 m and from 0.13 to 0.10 m, respectively, compared to the GE-DF solution. Also, the GC-TF model improves the 2D and 3D positioning precision from 0.10 to 0.08 m and from 0.14 to 0.12 m, respectively, with respect to the GC-DF model. Improvement in positioning precision is obtained from the GEC-TF processing model as well in comparison to the GEC-DF processing model by about 0.03 and 0.04 m in the 2D and 3D directions, respectively.

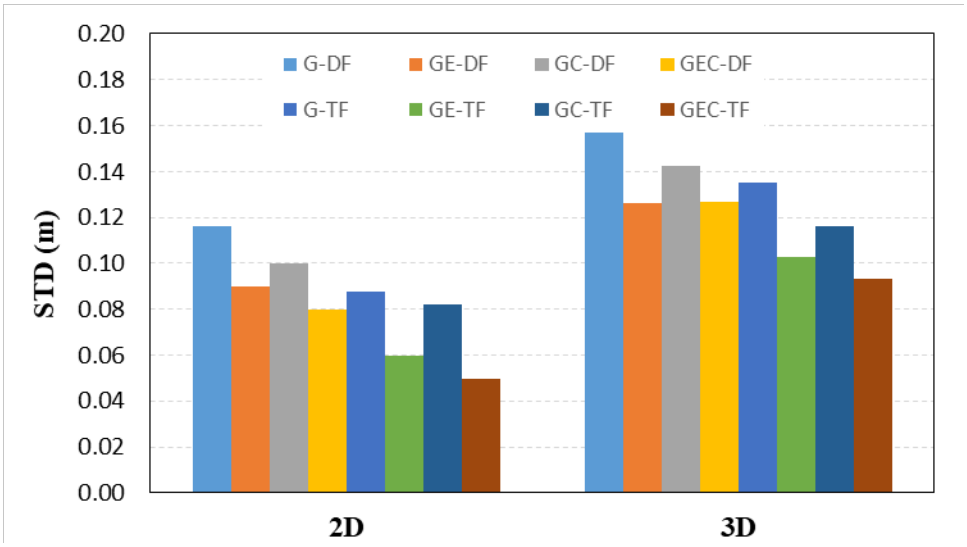

Figure 8. STD of the 2D position for the proposed PPP solutions

Furthermore, the statistical parameters for the 2D position including the mean and root mean square error (RMSE) are computed (Table 3) to assess the accuracy of the developed PPP solutions. As can be seen in Table 3, the 2D positioning accuracy is improved by adding the third frequency to the traditional dual-frequency PPP solutions. For example, the horizontal accuracy of the G-TF PPP solution is improved by about 37% compared to the G-DF PPP solution. The 2D position of the GE-TF PPP solution is also increased by about 22% compared to the GE-DF PPP solution. Enhancement in the 2D position is also obtained through the GEC-DF model by about 20% with respect to the GEC-DF model. An expectation is the GC-TF processing model. This might be attributed to the influence of the BeiDou L_1/L_3 IFB and ISB.

It is also shown that the 2D position accuracy of the triple-frequency PPP solutions is significantly enhanced compared to the widely used G-DF PPP processing model. For instance, the GE-TF PPP solution enhances the 2D position by about 55% in comparison to the G-DF PPP solution. Also, the horizontal positioning accuracy is improved by about 25% and 60% for GC-TF PPP and GEC-TIF PPP solutions, respectively, compared to the G-DF PPP solution.

Table 3. Statistical analysis of 2D position for different PPP solutions

PPP solution	Statistical parameter (m)		PPP solution	Statistical parameter (m)	
	Mean	RMSE		Mean	RMSE
G-DF	0.140	0.172	G-TF	0.107	0.109
GE-DF	0.084	0.099	GE-TF	0.073	0.078
GC-DF	0.097	0.115	GC-TF	0.123	0.129
GEC-DF	0.064	0.085	GEC-TF	0.092	0.068

To compare the accuracy of the proposed PPP solutions with the IMO requirements, RMSE of the horizontal positioning should be estimated at 95% confidence level as follows (El-Diasty and Elsobeiey, 2015):

$$RMSE_{95\%}^{2D} = 2.44 \times \sqrt{\frac{\sum_{m=1}^{n}(\Delta long_m^2 + \Delta lat_m^2)}{n}} \tag{20}$$

where $RMSE_{95\%}^{2D}$ is the root mean square error of the horizontal position at 95% confidence level; $\Delta long$ is the difference between the estimated longitudes from the PPP and differential solutions; Δlat is the difference between the estimated latitudes from the PPP and differential solutions; n is the total number of epochs. Then, the estimated RMSE is compared to the given absolute horizontal accuracy, as shown in Table 1. The integrity of the PPP solutions is also investigated for IMO standards. This is achieved through the comparison of the estimated epoch-by-epoch horizontal position with the integrity alert limit presented in Table 1. The computed maximum horizontal error should be less than the alert limit for a time duration of more than 3 h without any gap.

Table 4 summarizes the estimated RMSE of the 2D position at 95% confidence interval and maximum 2D positioning errors obtained from the proposed PPP solutions. It is found that, compared to Table 1, the positioning accuracy of the dual- and triple-frequency PPP solutions achieved the IMO requirements for ocean, coastal, port approach, port, inland waterways, and track control navigation applications. However, none of the proposed PPP solutions achieved the automatic docking navigation application. For the IMO integrity requirements, the proposed PPP solutions fulfilled the IMO requirements for all navigation phases. An exception is the GPS and GPS/BeiDou PPP solutions, which did not fulfill the automatic docking application.

Table 4. Maximum 2D position error and 2D RMSE at 95% confidence for the PPP solutions

PPP solution	Statistical parameter (m)		PPP solution	Statistical parameter	
	Maximum	$\mathbf{RMSE_{95\%}^{2D}}$		Maximum	$\mathbf{RMSE_{95\%}^{2D}}$
G-DF	0.346	0.420	G-TF	0.162	0.265
GE-DF	0.215	0.242	GE-TF	0.149	0.190
GC-DF	0.236	0.279	GC-TF	0.243	0.314
GEC-DF	0.168	0.221	GEC-TF	0.221	0.175

5. CONCLUSION

The performance of the triple-frequency quad-constellation kinematic PPP solution using real-time CNES products in maritime applications has been evaluated. The obtained kinematic PPP accuracy has been validated with respect to the IMO positioning accuracy and integrity

requirements. GPS/Galileo/BeiDou measurements have been collected from a moving vessel. Then, the observations have been processed using dual-frequency PPP and triple-frequency PPP solutions. Five satellite combinations have been considered namely, GPS-only, GPS/Galileo, GPS/BeiDou, and GPS/Galileo/BeiDou. The computed coordinates have been compared to those computed from the GPS-only differential solution. It has been found that the triple-frequency kinematic PPP accuracy has improved to be at a decimeter level compared to the dual-frequency PPP. In addition, the horizontal positioning accuracy has enhanced by about 37%, 55%, 25%, and 60% for the GPS-only, GPS/Galileo, GPS/BeiDou, and GPS/Galileo/BeiDou triple frequency PPP solutions, respectively, compared to the traditional GPS dual-frequency PPP solution. Furthermore, the IMO positioning accuracy requirement for ocean, coastal, port approach, port, inland waterways, and track control applications has been achieved by the proposed PPP solutions. The automatic docking application's accuracy requirement, however, has not been fulfilled by any PPP solution. The IMO integrity requirement also has been fulfilled by the PPP solutions for all navigation applications, except the GPS and GPS/BeiDou PPP solutions, which have not achieved the integrity requirement for automatic docking application only.

REFERENCES

Akplnar, B., Aykut, N. O. (2017). Determining the Coordinates of Control Points in Hydrographic Surveying by the Precise Point Positioning Method. *Journal of Navigation, 70*(6), 1241-1252.

Alkan, R. M., Erol, S., Ozulu, I. M., Ilci, V. (2020). Accuracy comparison of post-processed PPP and real-time absolute positioning techniques. *Geomatics, Natural Hazards and Risk, 11*(1), 178-190.

Alkan, R. M., Öcalan, T. (2013). Usability of the GPS precise point positioning technique in marine applications. *Journal of Navigation, 66*(4), 579-588.

Alkan, R. M., Saka, M. H., Ozulu, M., İlçi, V. (2017). Kinematic precise point positioning using GPS and GLONASS measurements in marine environments. *Measurement: Journal of the International Measurement Confederation, 109*, 36-43.

Berber, M., Wright, W. (2016). Online kinematic GNSS data processing for small hydrographic surveys. *Ocean Engineering, 112*, 335-339.

Cao, X., Li, J., Zhang, S., Kuang, K., Gao, K., Zhao, Q., Hong, H. (2019). Uncombined precise point positioning with triple-frequency GNSS signals. *Advances in Space Research, 63*(9), 2745-2756.

Chen, C., Xiao, G., Chang, G., Xu, T., Yang, L. (2021). Assessment of GPS/GALILEO/BDS precise point positioning with ambiguity resolution using products from different analysis centers. *Remote Sensing, 13*(16).

CNES (2023). Centre National d'Etudes Spatiales, http://www.ppp- wizard .net /products /REAL _TIME/. Accessed on January 1st, 2023.

El-Diasty, M. (2016). Development of Real-Time PPP-Based GPS/INS Integration System Using IGS Real-Time Service for Hydrographic Surveys. *Journal of Surveying Engineering, 142*(2), 05015005-05015005.

El-Diasty, M., Elsobeiey, M. (2015). Precise Point Positioning Technique with IGS Real-Time Service (RTS) for Maritime Applications. *Positioning, 06*(04), 71-80.

Elmezayen, A., El-Rabbany, A. (2021). Performance Assessment of Real-Time Multiconstellation GNSS PPP Using a Low-Cost Dual-Frequency GNSS Module. *Artificial*

Satellites, 56(3), 37-56.

Erol, S. (2020). A comparative study for performance analysis of kinematic multi-constellation GNSS PPP in dynamic environment. *Journal of Marine Science and Engineering, 8*(7), 1-19.

Erol, S., Alkan, R. M., Ozulu, M., İlçi, V. (2020). Performance analysis of real-time and post-mission kinematic precise point positioning in marine environments. *Geodesy and Geodynamics, 11*(6), 401-410.

Farah, A. (2018). Kinematic-PPP using Single/Dual Frequency Observations from (GPS, GLONASS and GPS/GLONASS) Constellations for Hydrography. *Artificial Satellites, 53*(1), 39-46.

Geng, J., Guo, J., Meng, X., Gao, K. (2020). Speeding up PPP ambiguity resolution using triple-frequency GPS/BeiDou/Galileo/QZSS data. *Journal of Geodesy, 94*(1).

Guo, F., Zhang, X., Wang, J., Ren, X. (2016). Modeling and assessment of triple-frequency BDS precise point positioning. *Journal of Geodesy, 90*(11), 1223-1235.

Guo, J., Geng, J., Wang, C. (2021). Impact of the third frequency GNSS pseudorange and carrier phase observations on rapid PPP convergences. *GPS Solutions, 25*(2).

Hofmann-Wellenhof, B., Lichtenegger, H., Walse, E. (2008). GNSS Global Navigation Satellite Systems: GPS, GLONASS, Galileo, and More. Springer, New York.

IGS (2023). International GNSS service, https://cddis.nasa.gov/archive/gnss/products/. Accessed on January 1st, 2023.

IMO (2002). International Maritime Organization. Revised maritime policy and requirements for a future GNSS. Resolution A.915(22). Available at https://wwwcdn.imo.org/localresources/en/KnowledgeCentre/IndexofIMOResolutions/AssemblyDocuments/A.915(22).pdf

Katsigianni, G., Loyer, S., Perosanz, F. (2019). PPP and PPP-AR kinematic post-processed performance of GPS-only, Galileo-only and multi-GNSS. *Remote Sensing, 11*(21).

Kazmierski, K., Zajdel, R., Sośnica, K. (2020). Evolution of orbit and clock quality for real-time multi-GNSS solutions. *GPS Solutions, 24*(4).

Li, P., Jiang, X., Zhang, X., Ge, M., Schuh, H. (2020). GPS + Galileo + BeiDou precise point positioning with triple-frequency ambiguity resolution. *GPS Solutions, 24*(3).

Naciri, N., Bisnath, S. (2021). Approaching global instantaneous precise positioning with the dual-and triple-frequency multi-GNSS decoupled clock model. *Remote Sensing, 13*(18).

Nie, Z., Liu, F., Gao, Y. (2020). Real-time precise point positioning with a low-cost dual-frequency GNSS device. *GPS Solutions, 24*(1).

Nie, Z., Wang, B., Wang, Z., He, K. (2020). An offshore real-time precise point positioning technique based on a single set of BeiDou short-message communication devices. *Journal of Geodesy, 94*(9).

Pan, L., Zhang, X., Liu, J. (2019). A comparison of three widely used GPS triple-frequency precise point positioning models. *GPS Solutions, 23*(4).

Rabbou, M. A., Abdelazeem, M., Morsy, S. (2021). Performance evaluation of triple-frequency gps/galileo techniques for precise static and kinematic applications. *Sensors, 21*(10).

Specht, C., Dabrowski, P. S., Pawelski, J., Specht, M., Szot, T. (2019). Comparative analysis of positioning accuracy of GNSS receivers of Samsung Galaxy smartphones in marine dynamic measurements. *Advances in Space Research, 63*(9), 3018-3028.

Tegedor, J., Ørpen, O., Melgard, T., Lapucha, D., Visser, H. (2017). G4 Multi-constellation Precise Point Positioning Service for High Accuracy Offshore Navigation. *TransNav, the International Journal on Marine Navigation and Safety of Sea Transportation, 11*(3), 425-429.

Tunalioglu, N., Ocalan, T., Dogan, A. H. (2022). Precise Point Positioning with GNSS Raw Measurements from an Android Smartphone in Marine Environment Monitoring. *Marine Geodesy*.

Wang, A., Chen, J., Zhang, Y., Meng, L., Wang, B., Wang, J. (2020). Evaluating the impact of CNES real-time ionospheric products on multi-GNSS single-frequency positioning using the IGS real-time service. *Advances in Space Research, 66*(11), 2516-2527.

Wang, Z., Li, Z., Wang, L., Wang, X., Yuan, H. (2018). Assessment of multiple GNSS real-Time SSR products from different analysis centers. *ISPRS International Journal of Geo-Information, 7*(3).

Yang, F., Zhao, L., Li, L., Feng, S., Cheng, J. (2019). Performance evaluation of kinematic BDS/GNSS real-time precise point positioning for maritime positioning. *Journal of Navigation, 72*(1), 34-52.

ZHANG, Y., CHEN, J., GONG, X., CHEN, Q. (2020). The update of BDS-2 TGD and its impact on positioning. *Advances in Space Research,* 65**,** 2645-2661.

Zhao, X., Ge, Y., Ke, F., Liu, C., Li, F. (2020). Investigation of real-time kinematic multi-GNSS precise point positioning with the CNES products. *Measurement: Journal of the International Measurement Confederation, 166*.

Received: *2023-01-14*

Reviewed: *2023-02-23 (undisclosed name); 2023-07-12 (undisclosed name); 2023-07-31 (undisclosed name)*

Accepted: *2023-10-24*